Controllable synthesis of graphene-based titanium dioxide nanocomposites by atomic layer deposition

2011 Nanotechnology 22 165602

(http://iopscience.iop.org/0957-4484/22/16/165602)

Nanotechnology **22** (2011) 165602 (10pp) doi:10.1088/0957-4484/22/16/165602

Controllable synthesis of graphene-based titanium dioxide nanocomposites by atomic layer deposition

Xiangbo Meng, Dongsheng Geng, Jian Liu, Ruying Li and Xueliang Sun[1]

Department of Mechanical and Materials Engineering, The University of Western Ontario, London, ON, N6A 5B8, Canada

E-mail: xsun@eng.uwo.ca

Received 29 December 2010, in final form 1 February 2011
Published 11 March 2011
Online at stacks.iop.org/Nano/22/165602

Abstract
Atomic layer deposition (ALD) was used to synthesize graphene-based metal oxide nanocomposites. This strategy was fulfilled on the preparation of TiO_2–graphene nanosheet (TiO_2–GNS) nanocomposites using titanium isopropoxide and water as precursors. The synthesized nanocomposites demonstrated that ALD exhibited many benefits in a controllable means. It was found that the as-deposited TiO_2 was tunable not only in its morphologies but also in its structural phases. As for the former, TiO_2 was transferable from nanoparticles to nanofilms with increased cycles. With regard to the latter, TiO_2 was changeable from amorphous to crystalline phase, and even a mixture of the two with increased growth temperatures (up to 250 °C). The underlying growth mechanisms were discussed and the resultant TiO_2–GNS nanocomposites have great potentials for many applications, such as photocatalysis, lithium-ion batteries, fuel cells, and sensors.

S Online supplementary data available from stacks.iop.org/Nano/22/165602/mmedia

(Some figures in this article are in colour only in the electronic version)

1. Introduction

Since the discovery of graphene in 2004 [1], many exceptional properties have been reported to date, such as high values of Young's modulus (∼1100 GPa) [2], fracture strength (125 GPa) [2], thermal conductivity (∼5000 W m^{-1} K^{-1}) [3], mobility of charge carriers (20 000 cm^2 V^{-1} s^{-1}) [4], and specific surface area (2630 m^2 g^{-1}) [5]. As a consequence, a vast amount of research has been stimulated to explore its applications in recent years. One possible way to utilize these properties in applications would be to incorporate graphene in composite materials. In this way, recently there was an increasing interest in using graphenes as building blocks in various composites and this kind of nanocomposites exhibited many benefits due to the combination of desirable properties of different materials. So far, graphene (or graphene stacks, a few layers of graphene) has been reported in the incorporation with three main types of materials: polymers [6–8], metals [9–11], and metal oxides [12–23], covering a series of applications (including field emitters, photocatalysis, conductors, supercapacitors, solar cells, fuel cells, batteries, etc) with improved mechanical, electrical, optical, or electrochemical properties. Of the aforementioned cases, metal oxide–graphene nanocomposites (MO–GNCs) represent an important class, mainly synthesized via solution-based methods. Although the solution-based methods offer potentially low cost and scalability, they are also exposed with inflexibility in precisely manipulating the deposition of metal oxides.

To circumvent the inability of the solution-based methods in precise synthesis, we fulfilled the preparation of MO–GNCs via a non-aqueous strategy, atomic layer deposition (ALD) in our recent work. ALD as a gas–solid synthesis route is featured by two sequentially cyclic self-limiting half-reactions, and by nature it is a layer-by-layer technique. In particular, the self-limiting characteristic distinguishes itself

[1] Author to whom any correspondence should be addressed.

from aqueous solution methods and other vapor deposition techniques (e.g., chemical and physical vapor deposition) in these ways: precise control in deposition at the atomic level, excellent uniformity and conformality of deposited materials. Since the beginning of the 21st century, ALD has been moving into a fashion for nanotechnology and expanding its uses from the deposition of simple two-dimensional (2D) planar films to the preparation of complex nanostructures of various materials [24, 25]. Additionally, ALD has the capability to deposit both inorganic (metals and metal oxides) and organic materials (polymers) [26]. Thus, ALD has potentials to provide many beneficial factors in synthesizing MO–GNCs by manipulating the deposition of MOs. Amongst the MO–GNCs reported in the literature, TiO_2–graphene nanocomposites are probably the most intensively investigated one, exhibiting improved performance in lithium-ion batteries (LIBs) [18], photocatalysis [19, 20], solar cells [21–23], etc. In earlier studies, TiO_2 in the forms of 2D planar films [27–34], 1D nanotubes [35–40], 0D composite nanoparticles [41, 42], and other complicated nanostructures [43] have been prepared by ALD. A variety of precursors were previously applied for various ALD-TiO_2 processes, but $TiCl_4$ and titanium isopropoxide (TTIP, $Ti(OCH(CH_3)_2)_4$) were two widely used titanium sources, and water was the most common oxygen source. In comparison, TTIP and water as the ALD precursors had one main advantage over the use of $TiCl_4$ and water: no release of the corrosive by-product HCl and no chlorine residues in the film [27, 30].

To date, however, there was little effort in developing TiO_2–GNCs via ALD yet. Thus, in our recent attempts TiO_2 was chosen as the candidate and deposited on graphene nanosheet (GNS) powders (synthesized in our group) using TTIP and water as the ALD precursors. The success of the synthesis of TiO_2–GNS nanocomposites demonstrated that the ALD approach exhibited many advantages by controlling the deposition of TiO_2. First of all, in contrast to the solution-based methods employed in reported work [18–23], the ALD method could synthesize nanocomposites with the TiO_2 component precisely controlled in its morphologies as well as contents by changing ALD cycles. In addition, it was for the first time found that the as-deposited TiO_2 could be tuned in structures from amorphous to crystalline anatase phase by simply adjusting growth temperatures. In particular, the growth temperature for the deposited anatase TiO_2 is only around 250 °C, which has not been reported in earlier studies. Consequently, this work provided not only an alternative approach to synthesize MO–GNCs but multiple choices of MO–GNCs as well. The resultant nanocomposites have great potentials for many important applications.

2. Experimental details

2.1. Preparation of GNS

For preparation of GNS, we first oxidized natural graphite (NG) powder (45 μm, 99.99%, Sigma-Aldrich, as shown in figure SI-1(a), supporting information available at stacks.iop.org/Nano/22/165602/mmedia) using a modified Hummers method [44]. In detail, graphite powder (1 g) was first stirred in concentrated sulfuric acid (23 ml) with a sunsequent addition of sodium nitrate (0.5 g) at room temperature. The stirring lasted for 16 h, and then the mixture was cooled down to 0 °C. Thereafter, potassium permanganate (3 g) was added to form a new mixture. Two hours later, the mixture became a green paste at around 35 °C and was stirred for another 3 h. Then, water (46 ml) was slowly added to the paste and the temperature was increased to 98 °C. The suspension remained at this temperature for 30 min before it was further diluted with another addition of water and hydrogen peroxide (140 ml). Following this, the suspension was filtered and washed until the pH value of the filtrate was neutral. The as-received slurry is the so-called graphite oxide (GO, figure SI-1(b), supporting information available at stacks.iop.org/Nano/22/165602/mmedia), which was further dried in a vacuum oven at 60 °C. Further, the as-synthesized GO was first flushed by Ar for 20 min in a quartz tube. Then, the quartz tube was promptly moved into a Lindberg tube furnace with a preheated temperature around 1050 °C. After 30 s thermal treatment, GO was reduced into expanded GNS powders (figure SI-1(c), supporting information available at stacks.iop.org/Nano/22/165602/mmedia).

2.2. ALD-TiO_2

In ALD-TiO_2 processes, the as-prepared GNS powders were first loaded into a commercial ALD reactor (Savannah 100, Cambridge Nanotechnology Inc., USA) preheated to a certain temperature. Then, TTIP (98%, Sigma-Aldrich) and deionized water (DI H_2O) were introduced into the ALD reactor in an alternating sequence to perform ALD-TiO_2. TTIP was heated to 70 °C while water was kept at room temperature in order to provide sufficient vapors for ALD-TiO_2 processes. Additionally, the delivery lines were heated to 150 °C in order to prevent the precursors from condensing. Nitrogen was used as the carrier gas with a flow rate of 20 sccm and the ALD reactor was sustained at a low level of pressure (typically 0.4 Torr) with a vacuum pump (Pascal 2005 I, Adixon). The ALD procedures were set as follows: (1) a 1.0 s supply of TTIP; (2) a 3.0 s extended exposure of TTIP to GNS; (3) a 10.0 s purge of oversupplied TTIP and any by-products; (4) a 2.0 s supply of water vapor; (5) a 3.0 s extended exposure of water vapor to GNS; (6) a 10.0 s purge of oversupplied water and any by-products. The aforementioned six-step sequence constituted one ALD-TiO_2 cycle and the ALD processes could be adjustable with different cycling numbers and growth temperatures. In this study, three growth temperatures were employed for ALD-TiO_2 processes: 150, 200, and 250 °C.

2.3. Characterization

To characterize the morphologies, structures, and compositions of various samples, we used field emission scanning electron spectrometry (FE-SEM, Hitachi 4800S) coupled with energy dispersive spectroscopy (EDS), transmission electron microscopy (TEM, Philips CM10), high-resolution TEM (HRTEM, JEOL 2010 FEG), x-ray diffractometry (XRD, Intel multi-purpose diffractometer), and Fourier transform infrared spectroscopy (FTIR, Bruker Tensor 27).

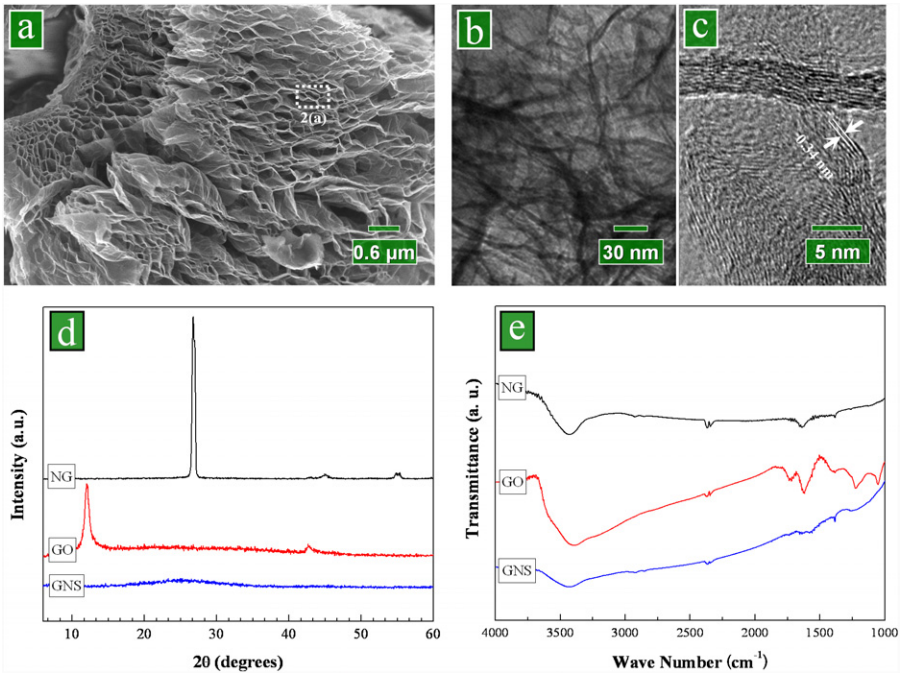

Figure 1. (a) SEM images of GNS; (b) TEM image, and (c) HRTEM image of GNS; (d) XRD and (e) FTIR spectra of NG, GO, and GNS.

3. Results and discussion

3.1. Results

As stated above, GNS was made from GO (the products of oxidized NG) and used as the building block in synthesizing MO–GNCs. The characteristics of GNS were characterized by employing SEM, TEM, XRD, and FTIR, as illustrated in figure 1. In contrast to its starting materials NG (figure SI-1(a) available at stacks.iop.org/Nano/22/165602/mmedia) and GO (figure SI-1(b) available at stacks.iop.org/Nano/22/165602/mmedia), GNS (the SEM image in figure 1(a)) presents a fluffy and porous structure [45] featuring numerous honeycombs. The honeycombs are surrounded by graphene wrinkles. The TEM image in figure 1(b) confirms the interlinked nature of the wrinkles. The HRTEM image in figure 1(c) further reveals that the wrinkles consist of several graphene layers (typically fewer than 10 layers), i.e., graphene stacks. The interlayer distance is 0.34 nm. XRD spectra (figure 1(d)) clearly distinguish the as-synthesized GNS from its starting materials, NG and GO. NG has the strongest (002) peak at 26.8°, but GO shows the strongest (001) diffraction peak at 12°, suggesting that the interlayer distance increased and the structure was modified due to oxygenated groups [46]. In contrast, GNS receives a broad diffraction (002) peak shifted back to 26.8°, implying that GO was reduced via the rapid thermal expansion and the extensive conjugated sp^2 carbon network (i.e., the ordered crystal structure) was restored [47]. FTIR spectra (figure 1(e)) further demonstrate the evolution of functional groups from NG to GO and GNS. NG mainly shows the stretching vibrations of hydroxyl (–OH) groups (3420 cm^{-1}) and C=C (1586 cm^{-1}) [48–50]. Besides the aforementioned groups, the GO spectrum is added with the stretching vibrations of C=O (1736 cm^{-1}), carboxy C–O (1414 cm^{-1}), epoxy C–O (1220 cm^{-1}), and C–O (1100 cm^{-1}) [48–50]. In comparison, GNS mainly has the stretching vibrations of hydroxyl groups and C=C [48–50]. The FTIR spectra imply that GNS was significantly reduced. Peaks below 900 cm^{-1} are usually not interpreted for they represent too complex a structural signature [46].

ALD-TiO_2 was performed on the as-prepared GNS powders with a series of cycles under three growth temperatures (150, 200, and 250 °C). The as-synthesized nanocomposites received from 300-cycle ALD-TiO_2 were characterized and compared, as shown in figure 2. It was found that growth temperature evidently influenced the natures of the as-synthesized nanocomposites. Figure 2(a) shows a high-magnification SEM image for a local area of GNS, and its location is indicated in the inset of figure 2(a) as well as in figure 1(a). Obviously, the wrinkles are very thin (less than 3.4 nm in most cases, as disclosed in figure 1(c)). In contrast, a 300-cycle ALD-TiO_2 process changed the morphologies of GNS significantly, as shown in figures 2(b)–(d) and their insets with the same magnification. Remarkably, the wrinkles became thicker to around 15 nm (figure 2(b)), 29 nm (figure 2(c)), and 18 nm (figure 2(d)), corresponding to the growth temperature of 150, 200, and 250 °C, respectively. Obviously, ALD-TiO_2 deposited a layer of film on GNS in all the cases, which differed in thickness with temperature. Furthermore, if we suppose the pristine graphene wrinkles are around 3.4 nm with a conservative estimate, the average growth rates (or the growth per cycle, GPC) would be roughly evaluated as 0.19, 0.43, and 0.24 Å/cycle, respectively. The calculation of GPC is based on the homogeneous nature of ALD deposition on both sides of wrinkles and can be expressed by an equation: GPC = (thickness of coated wrinkles − thickness of pristine

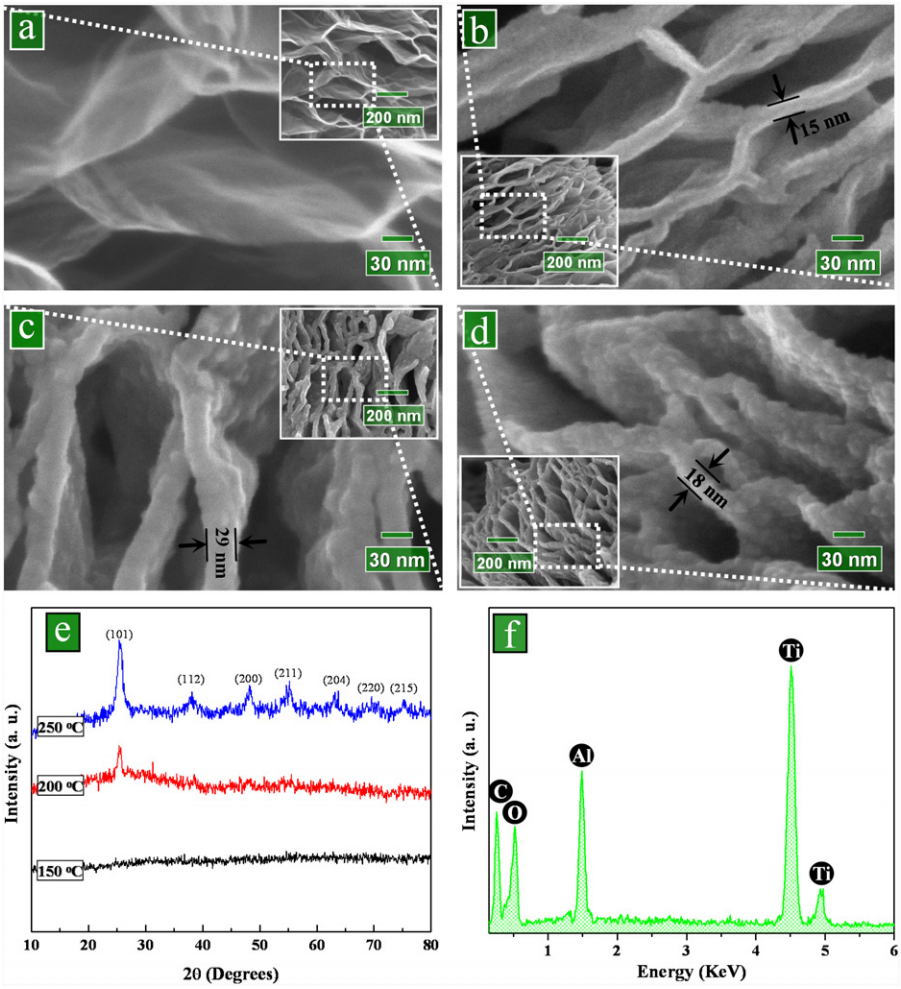

Figure 2. High-magnification SEM images of (a) pristine GNS, and 300-cycle ALD-TiO_2 on GNS at (b) 150 °C, (c) 200 °C, and (d) 250 °C. Insets are low-magnification SEM images. (e) XRD spectra of 300-cycle ALD-TiO_2 on GNS at 150, 200, and 300 °C. (f) EDS spectra of 300-cycle ALD-TiO_2 on GNS at 150 °C.

wrinkles)/(2 × cycling numbers). Nevertheless, it was worth noting that the as-deposited TiO_2 is morphologically different under the three growth temperatures. In the case of 150 °C (figure 2(b)), the as-deposited layer is uniform and smooth; in the case of 200 °C (figure 2(c)), the deposited layer is mainly smooth except for some nanoparticles of around 15 nm which protrude from the film; in the case of 250 °C (figure 2(d)), however, the deposited layer becomes totally rough and bumpy. Thus, we postulated that growth temperature had influenced not only the deposition rates but the structures of the as-deposited TiO_2 as well. As for the latter one, XRD results illustrated in figure 2(e) provide the evidence. No peaks are identified with the sample deposited at 150 °C, suggesting that the as-deposited TiO_2 is amorphous. However, the sample grown at 200 °C exhibits a significant peak at 25.28° as well as two weak but uncertain peaks at 38.58° and 48.05°, corresponding to the (101), (112), and (200) planes of anatase TiO_2 (JCPDS PDF No 21-1272), respectively. Furthermore, the XRD spectra of the sample grown at 250 °C present more peaks with increased intensities, corresponding to different characteristic planes of anatase TiO_2 (JCPDS PDF No. 21-1272) as denoted in figure 2(e). Obviously there existed phase transitions in the growth of ALD-TiO_2 with temperature. In addition, the compositions of the sample grown at 150 °C were further investigated using EDS, as shown in figure 2(f). Besides the confirmation on the presence of C, Ti, and O, figure 2(f) also shows some Al element contributed by the Al sample holder. Based on the information disclosed by figure 2, it is clearly shown that the growth temperatures influenced the structural phases, morphologies, and deposition rates of the as-grown TiO_2. For more detailed growth characteristics, we examined the evolution of the ALD-TiO_2 with increasing number of ALD cycles in each case.

Figure 3 reveals the growth of ALD-TiO_2 at 150 °C. A 50-cycle ALD-TiO_2 process (figure 3(a)) covered GNS with tiny nanoparticles of 2–3 nm uniformly and the nanoparticles grew to around 5 nm (the inset of figure 3(b)) with an additional 25 cycles (figure 3(b)). After a 100-cycle ALD-TiO_2 (figure 3(c)), a film was fully formed on GNS with a little roughness and the wrinkles expose a thickness of around 7 nm. With another addition of 100 cycles (figure 3(d)), the film became smoother and much thicker. The wrinkles unveil a thickness of around 11 nm. Combined with the information of 300-cycle ALD-TiO_2 revealed in figure 2(b), we conclude

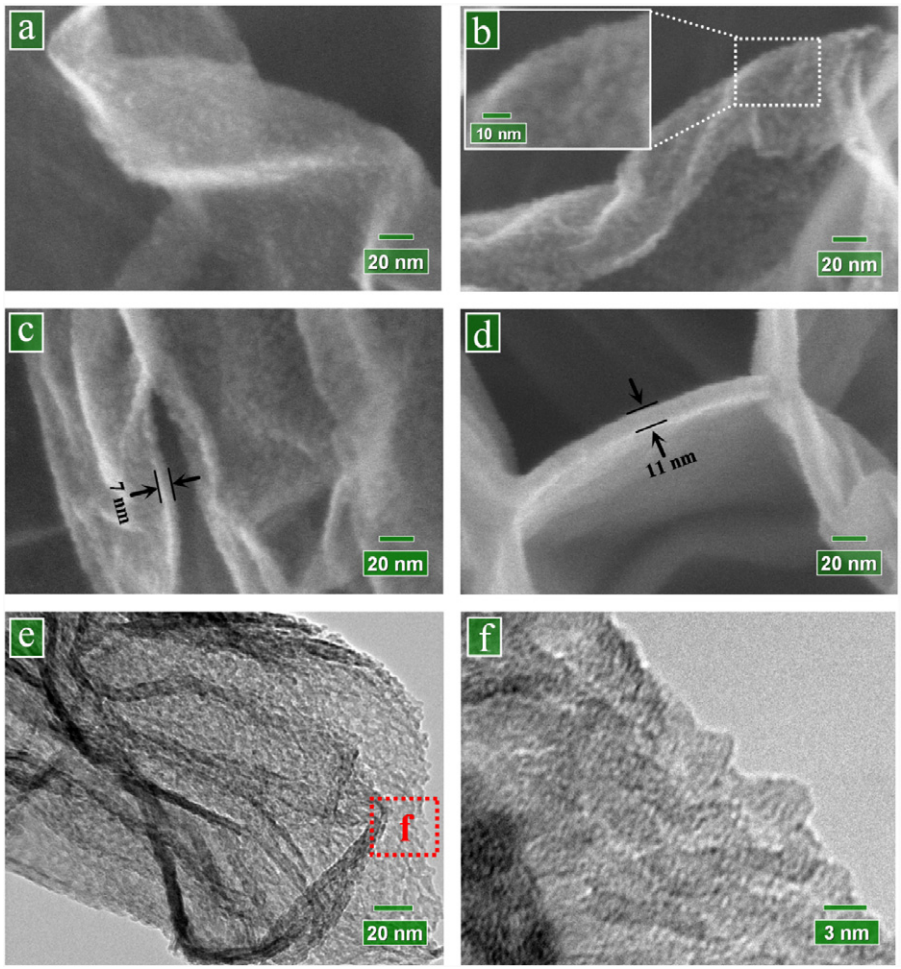

Figure 3. High-magnification SEM images of ALD-TiO_2 on GNS at 150 °C after (a) 50 cycles, (b) 75 cycles (inset for a higher magnification SEM image), (c) 100 cycles, and (d) 200 cycles. (e) TEM and (f) HRTEM image of 75-cycle ALD-TiO_2 on GNS at 150 °C.

that the ALD-TiO_2 at 150 °C experienced a slower growth in the first 100 cycles, accounting for about 0.18 Å/cycle, and the growth rate was increased to a consistent rate of 0.2 Å/cycle after the first 100 cycles. More information is included in figure SI-2 in supporting information (available at stacks.iop.org/Nano/22/165602/mmedia). In addition, TEM and HRTEM were applied to examine a sample coated by a 75-cycle ALD-TiO_2. In figure 3(e), TEM observation confirms the information disclosed by SEM in figure 3(b). Additionally, we noticed that nanoparticles were going to coalesce into a full layer. A local area in the red square marked 'f' was further examined by HRTEM and shown in figure 3(f). The HRTEM image shows the disordered nature of the deposited TiO_2, providing additional evidence that the as-deposited TiO_2 was amorphous in structure. This is consistent with the XRD spectra for 150 °C in figure 2(e).

In figure 4, the growth of ALD-TiO_2 at 200 °C is illustrated. Similar to the case of 150 °C, GNS was mainly covered by nanoparticles after the first 50 and 75 cycles, as shown in figures 4(a) and (b), respectively. Upon finishing a 100-cycle ALD-TiO_2 (figure 4(c)), a significant change is observed from the thickness of the wrinkles, accounting for 11 nm typically. It is also observed that a smooth film has been formed on GNS. In addition, it is noticed that some particles (around 5 nm) stand out of the film, as white-circled in figure 4(c). While the ALD-TiO_2 proceeded to 200 cycles (figure 4(d)), we can see that the GNS wrinkles increased to around 20 nm and the protruding particles became bigger in size to around 10 nm. Combined with the information of the 300-cycle ALD-TiO_2 revealed in figure 2(c), it is easy to conclude that the ALD-TiO_2 at 200 °C also experienced a slower growth in the first 100 cycles, accounting for about 0.38 Å/cycle; and the growth rate was increased to a constant rate of 0.45 Å/cycle after the first 100 cycles. More information is included in figure SI-3 in supporting information (available at stacks.iop.org/Nano/22/165602/mmedia). Based on a sample with a 75-cycle ALD-TiO_2, the TEM image in figure 4(e) reveals that the nanoparticles are around 10 nm and almost coalesce into a film. HRTEM observation on a local area, in the red square marked 'f' in figure 4(e), is shown in (f). It is found that the as-deposited TiO_2 is mostly amorphous but decorated with some tiny crystalline nanoparticles of 2–3 nm, which are partially indicated by the white-circled areas in figure 4(f). The crystalline particles are identified with an

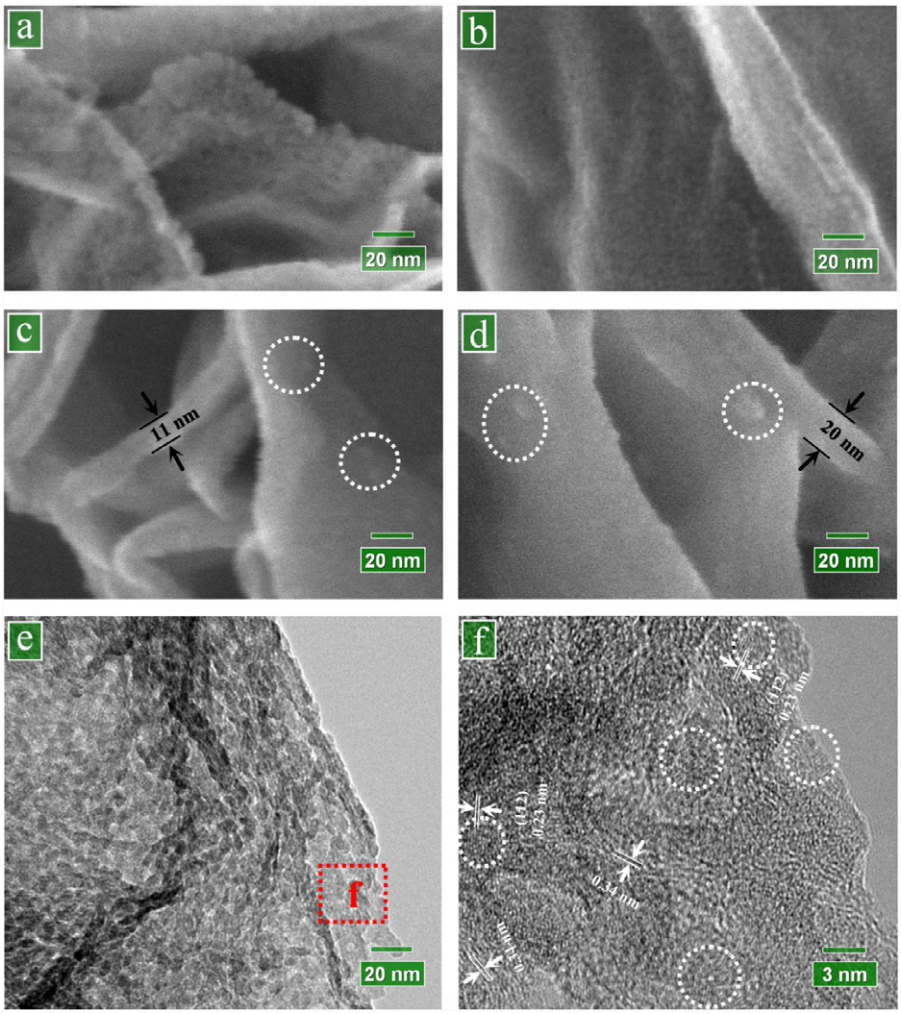

Figure 4. High-magnification SEM images of ALD-TiO_2 on GNS at 200 °C after (a) 50 cycles, (b) 75 cycles, (c) 100 cycles, and (d) 200 cycles. (e) TEM and (f) HRTEM image of 75-cycle ALD-TiO_2 on GNS at 200 °C.

inter-plane spacing of 0.23 nm, corresponding to the (112) planes of anatase TiO_2. In addition, the graphene lattices are also observable, as marked with a 0.34 nm inter-plane spacing in figure 4(f). Based on the above discussion, we could further conclude that the particles protruding from the films in figures 4(c) and (d) as well as in figure 2(c) are crystalline anatase while the films are mostly amorphous. Thus, we could know that the XRD spectra for 200 °C (figure 2(e)) resulted from the mixed amorphous and anatase phase of the as-deposited TiO_2. More specifically, the films are dominated by amorphous TiO_2 while the embellished anatase nanoparticles are responsible for the XRD characteristic peaks in figure 2(e).

Following the afore-discussed cases at 150 and 200 °C, we further demonstrate the growth of ALD-TiO_2 at 250 °C in figure 5. Firstly, the ALD-TiO_2 deposited nanoparticles in the first several tens of cycles, growing larger with increased cycles. In figure 5(a), the nanoparticles are less than 5 nm after a 50-cycle ALD-TiO_2. Figure 5(b) shows that the nanoparticles were significantly improved in their density while their sizes were increased to around 5 nm after a 75-cycle ALD-TiO_2. Upon finishing a 100-cycle ALD-TiO_2, the SEM image in figure 5(c) presents a layer of a rough film due to the coalescence of the nanoparticles. At this stage, the wrinkles with the sample show a thickness of around 8 nm. Moreover, the SEM image in figure 5(d) discloses that the wrinkles further grew in thickness to around 13 nm and the film retained some roughness. Combined with the information of the 300-cycle ALD-TiO_2 revealed in figure 2(d), it is obvious that ALD-TiO_2 at 250 °C experienced a slower growth of 0.23 Å/cycle in the first 100 cycles while almost remaining at a constant rate of 0.25 Å/cycle in the following cycles. More information is included in figure SI-4 in supporting information (available at stacks.iop.org/Nano/22/165602/mmedia.) Furthermore, based on a sample coated by a 75-cycle ALD-TiO_2, the TEM image in figure 5(e) confirms that the as-deposited nanoparticles are around 5 nm and are retained individually. HRTEM observation on a local area of figure 5(e) (in the red square marked 'f') is shown in figure 5(f). It reveals that all the as-deposited TiO_2 nanoparticles are crystalline and they mostly show an inter-plane spacing of 0.23 nm, corresponding to the (112) planes of anatase TiO_2. This is consistent with the XRD characteristic peak at 38.58° disclosed in figure 2(e) for 250 °C.

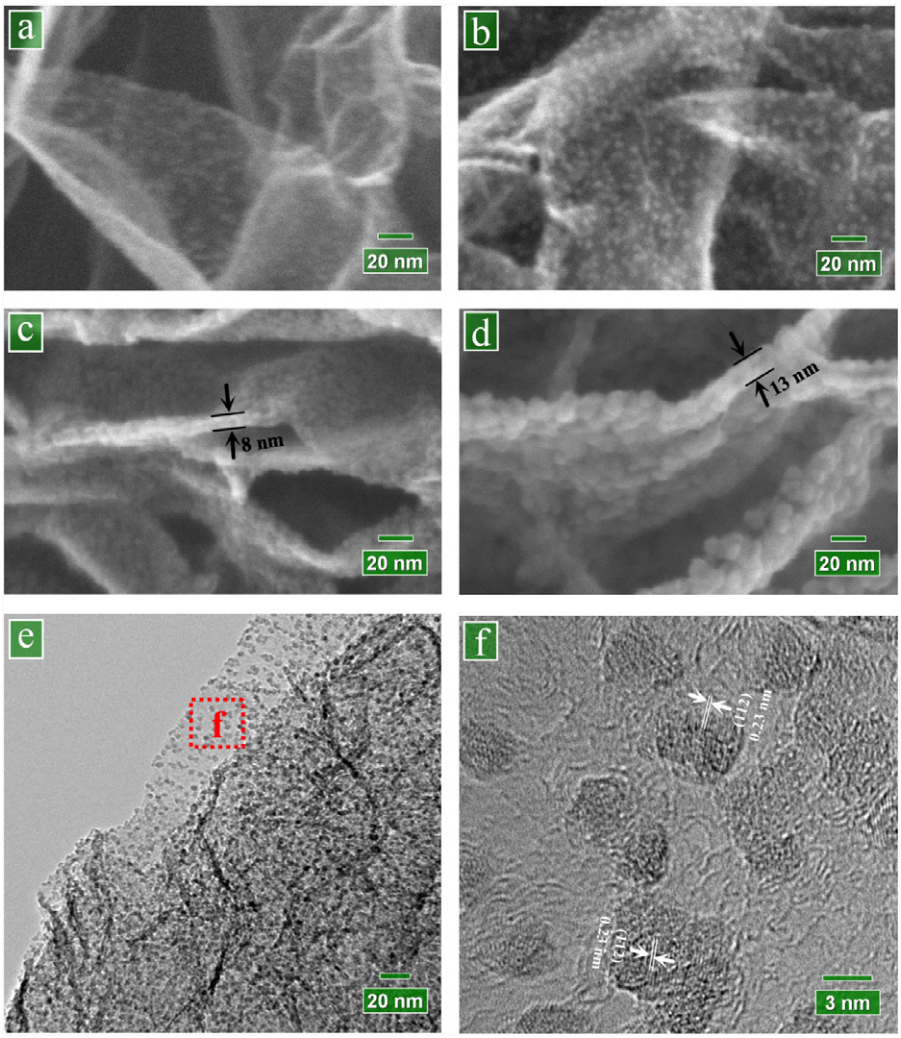

Figure 5. High-magnification SEM images of ALD-TiO_2 on GNS at 250 °C after (a) 50 cycles, (b) 75 cycles, (c) 100 cycles, and (d) 200 cycles. (e) TEM and (f) HRTEM image of 75-cycle ALD-TiO_2 on GNS at 250 °C.

3.2. Discussion

Based on the results disclosed above, one can easily learn that ALD as a strategy is flexible and precise in synthesizing MO–GNCs. In terms of the as-deposited TiO_2, its advantages are mainly exhibited in two ways: (1) tunable morphologies from nanoparticles to nanofilms; and (2) controllable structures from amorphous to crystalline anatase phase. The former is simply ascribed to its self-limiting and cyclic characters while the latter discloses the temperature-dependent nature of the ALD-TiO_2. To gain a better understanding, therefore, it is essential to clarify the determinant factors and to further explore the underlying mechanisms, which will be discussed in this section.

It is easy to understand that any result occurs only under suitable conditions. In ALD processes, generally, there are three key parameters: the precursors, substrates and temperatures [51]. As stated at the beginning of this study, TTIP and water were the precursors and GNS was used as the substrate for ALD-TiO_2. As for the growth temperatures, we applied ones not higher than 250 °C. On the choice of temperatures, it is in essence determined by the fundamentals of ALD as well as the properties of precursors. As a layer-by-layer deposition technique, ALD requires that the precursors will not decompose by themselves under a given growth temperature [27, 52]. Otherwise, the deposition will be a process of chemical vapor deposition (CVD), and destroy the self-limiting growth mechanism of ALD. Of the two precursors (TTIP and water), it is obvious that water being an oxygen source is not an issue for ALD-TiO_2 processes and it has been used at temperatures up to 600 °C [53]. The limit is mainly from TTIP. Some pioneer work conducted by Finnish researchers [27–29] has disclosed that TTIP is only chemically stable at temperatures not higher than 250 °C. Thus, any higher temperature would incur an increasing fraction of CVD growth of TiO_2 due to the decomposition of TTIP. Obviously, our experiments fell into a range of temperatures that were safe for the ALD processes of TiO_2.

In addition, in order to fulfill well the self-limiting layer-by-layer nature of the ALD technique, one needs to guarantee that there are sufficient vapors of the applied precursors supplied during ALD processes. Otherwise, a slower but uncertain growth [51] as well as some unexpected

structure [54] might be produced. Thus, to avoid these uncertainties, we investigated suitable pulse lengths for the precursors of TTIP and water. It was found that 0.8 s TTIP and 1.0 s water could provide sufficient vapors for an unchanged growth mode of the ALD-TiO_2. The evidence is included in figure SI-5 and 6 in the supporting information (available at stacks.iop.org/Nano/22/165602/mmedia). Therefore, the adopted pulses of 1.0 s TTIP and 2.0 s water in this study would always contribute a consistent deposition behavior of the ALD-TiO_2 for a certain temperature.

To further understand the findings disclosed in this study, one needs to know the roles played by the aforementioned parameters, which are associated with surface chemistry. It is well known that ALD as a surface-controlled process relies on two alternating half-reactions to realize a layer-by-layer deposition. Ascribed to Rahtu and Ritala [29], the ALD process of using TTIP and water was described by two half-reactions as follows:

$$2\|\text{–OH} + \text{Ti(OCH(CH}_3)_2)_4\ (\text{g}) \rightarrow \|\text{–O}_2\text{–Ti(OCH(CH}_3)_2)_2 + 2(\text{CH}_3)_2\text{CHOH (g)} \quad (1a)$$

$$\|\text{–O}_2\text{–Ti(OCH(CH}_3)_2)_2 + 2\text{H}_2\text{O(g)} \rightarrow \|\text{–O}_2\text{– Ti(OH)}_2 + 2(\text{CH}_3)_2\text{CHOH (g)} \quad (1b)$$

where the symbol '‖' denotes the substrate surface and '(g)' refers to gas phase species. In particular, Rahtu and Ritala claimed that this mechanism is suitable for an ALD-TiO_2 with a temperature not higher than 250 °C. Obviously, the self-limiting nature of (1*a*) and (1*b*) determines the precise growth of TiO_2. Due to its surface-controlled character, ALD requires a substrate functionalized for its initiation. To meet this requirement, the FTIR spectra of figure 1(e) clearly reveal that the as-prepared GNS was decorated with hydroxyl groups, which could initiate an ALD-TiO_2 by following the reaction of (1*a*).

Based on the above discussion, we will first clarify the facts on the tunable morphologies of the as-deposited TiO_2. As we observed, the as-deposited TiO_2 differed in morphologies and growth rates between the stage of the first 100 cycles and the stage after the first 100 cycles. To facilitate the following discussion, we refer them to stage I and stage II, respectively. In stage I, the as-deposited TiO_2 showed an island-like growth and appeared in the forms of nanoparticles with a lower growth rate; while in stage II, the as-deposited TiO_2 coalesced into nanofilms with a higher and constant growth rate. These serve for all the cases of different temperatures. As for the growth rates, we illustrated the values of GPC in figure 6. According to earlier studies, there are two potential reasons for the occurrence of stage I: steric hindrance of ligands and low density reactive surface sites [51]. Steric hindrance of ligands might cause the chemisorbed intermediates to shield part of the surface from being accessible to the precursors, depending strongly on the sizes of the surface intermediates. In the case of TTIP, the effective diameter of a molecule is significantly larger than that of a Ti or O site [28]. On the other hand, the low density of reactive sites provides fewer 'seats' than the numbers required for the precursors to bond and thereby to cover the surface. Thus, both could induce a low growth rate of TiO_2. When a film was fully formed on the surface

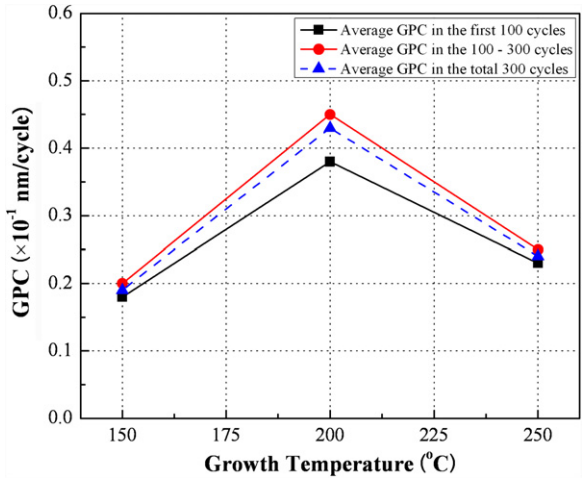

Figure 6. The growth rates (GPC) of ALD-TiO_2 with temperatures.

of GNS (i.e., in stage II), it is obvious that there would be more reactive sites. The increased reactive sites would promote the growth rates, as illustrated in figure 6. Quite clearly, the ALD-TiO_2 on GNS experienced a substrate-inhibited growth of type 1 [51]. Additionally, figure 6 also shows that, besides the effect of the cycling numbers, the growth of ALD-TiO_2 is also highly temperature dependent. In terms of the average GPC over the total 300 cycles, GPC increases with an increase in temperature from 150 to 200 °C, whereas it decreases with a further increase to 250 °C. To interpret this phenomenon, there are two factors for consideration: reactivity of precursors and density of reactive sites [51]. Aarik *et al* [28] revealed that water has a low reactivity towards TTIP in ALD-TiO_2, but an increase in growth temperature could improve the reactivity of water, activate some reactions, and thereby improve the growth rate of ALD-TiO_2. However, the increased temperatures might incur an unfavorable effect at the same time: dehydroxylation of hydroxyl groups [55], whose occurrence would change the surface reactivity of GNS and thereby influence the following deposition of TiO_2 towards the chemisorbed TTIP molecules. The dehydroxylation is described as follows [54]:

$$2\|\text{–OH} \rightarrow \| = \text{O} + \text{H}_2\text{O (g)}. \quad (2)$$

Remarkably, this dehydroxylation would reduce the number of hydroxyl groups and thereby lead to a lower growth rate. Thus, an increased temperature might exert two contrary effects on the ALD-TiO_2. As a consequence, the highest GPC would be achieved at a temperature at which a compromise could be reached between the two factors. It is easy to conclude that, as shown in figure 6, the improved GPC with an increased temperature from 150 to 200 °C was due to the predominance of the promoted reactivity of water while the reduced GPC with a further increase to 250 °C was induced by the dominant dehydroxylation. In addition, the evidence is also clearly shown in figures 3–5. For example, comparing figures 4(e) with 5(e), we can easily observe the reduced coverage due to dehydroxylation when the temperature was increased from 200 to 250 °C. Thus, the tunable morphologies of the as-deposited

TiO_2 were commonly determined by both the surface nature of the substrate and the applied temperature.

Besides tunable morphologies, it is of great interest to explain another main finding revealed in this study: the controllable structures of the as-deposited TiO_2 with growth temperature. In particular, this was rarely reported in the literature on using TTIP and water as the precursors. In earlier studies, TTIP and water had been used to fulfill the ALD-TiO_2 on a series of substrates (soda lime glasses [27, 29], silica substrates [28], silicon substrates [28, 30], nanoporous templates [35–37], and nanoparticles [42]) for various nanostructures. All the efforts exclusively contributed the deposition of amorphous TiO_2, except for a partial crystalline film grown on glasses at the temperature of 250 °C and at higher ones [27]. It is worth noting that we reveal a pure crystalline TiO_2 deposited on GNS (as demonstrated in figures 2 and 5) at 250 °C. Thus, it is necessary to explore the bases for its occurrence. In this way, previous studies demonstrated that, in manipulating the phase-controllable growth of TiO_2, both growth temperatures and substrates are important for the given precursors. Using $TiCl_4$ and water as ALD precursors, for example, amorphous TiO_2 films were grown on glasses while crystalline films were deposited on crystalline substrates under the same conditions [53]. Similarly, Schuisky *et al* also demonstrated that substrates could influence the structural phases of the as-deposited TiO_2 using TiI_4 and H_2O_2 as ALD precursors [56]. Nevertheless, Aarik *et al* [57] revealed that growth temperature is another important factor influencing the structural phases of TiO_2 using $TiCl_4$ and water as ALD precursors and higher temperatures are preferable to the growth of crystalline films on silicon substrates. Thus, it is reasonably believed that the characters of the as-prepared GNS and a relatively high temperature (250 °C) jointly contributed the crystalline anatase TiO_2 deposited on GNS in this work. First, a higher temperature (250 °C) should be kinetically favorable for the ordering of the structure with minimum energy [57], for the intermediates might be able to migrate easily and enable the Ti and/or O ions to occupy the positions corresponding to the lowest free energy of the crystal. Furthermore, GNS is crystalline by nature and this might have prompted the deposition of the pure anatase TiO_2 as well, as demonstrated on crystalline substrates using $TiCl_4$ and water in the literature [53]. In addition, a higher temperature (250 °C) might change the surface characters of GNS and the following deposition behaviors of the ALD-TiO_2 by modifying their reactive sites and natures. As a result, they might have been changed to be favorable for the preparation of the crystalline TiO_2. Unfortunately, there is to date little knowledge to interpret the roles of substrates in the literature and a further investigation on the growth mechanisms is needed. In comparison, two reasons might lead to previous failures in direct ALD-TiO_2 of crystalline structures using TTIP and water: low growth temperatures [35–37] or unfavorable substrates [27–30, 42]. As for the amorphous and mixed phases disclosed in figures 3 and 4 respectively, their lower temperatures ($\leqslant$200 °C) should be the most dominant factor.

In summary, we produced a series of MO–GNCs via ALD-TiO_2 using TTIP and water as precursors in this work and the as-synthesized TiO_2–GNS nanocomposites exhibited many peculiarities in a controllable means. Besides the tunable morphologies, the as-deposited TiO_2 was also controllable in structure. In addition to the self-limiting and cyclic natures of ALD, the precursors, temperatures, and substrate (GNS) are believed to be among the main factors, and their roles were discussed.

4. Conclusions

This work fulfills and exemplifies a non-aqueous approach to synthesize MO–GNCs. Based on powder-based GNS, TiO_2 was deposited on graphene (or graphene stacks) by ALD with a series of cycles at different temperatures. The results revealed that the as-synthesized TiO_2–GNS nanocomposites could be tuned in morphology as well as structure. As for the controllable structures of TiO_2, it is found that a lower temperature (150 °C) contributed to amorphous TiO_2 while a higher temperature (250 °C) produced crystalline anatase TiO_2. In particular, a phase transition was observed with an intermediate temperature (200 °C). In all the cases, by adjusting their cycling numbers, the as-deposited TiO_2 could present nanoparticles or nanofilms on GNS. Furthermore, we discussed and explained the underlying mechanisms responsible for both the controllable structures and morphologies of the as-synthesized TiO_2–GNS nanocomposites. As a consequence, this paper demonstrated that, in comparison to the solution-based methods exposed in the literature, ALD contributed a precise and flexible route to prepare MO–GNCs. The as-synthesized hybrid TiO_2–GNS materials are potentially important candidates for many important applications, such as lithium-ion batteries, solar cells, gas-sensing, and photocatalysis.

Acknowledgments

This research was supported by the Natural Science and Engineering Research Council of Canada (NSERC), the Canada Research Chair (CRC) Program, the Canadian Foundation for Innovation (CFI), the Ontario Research Fund (ORF), the Early Researcher Award (ERA) and the University of Western Ontario. In addition, the authors appreciate the help from Mr Fred Pearson in HRTEM analysis at the Canadian Center for Electron Microscopy, McMaster University.

References

[1] Novoselov K S, Geim A K, Morozov S V, Jiang D, Zhang Y, Dubonos S V, Grigorieva I V and Firsov A A 2004 *Science* **306** 666–9
[2] Lee C, Wei X, Kysar J W and Hone J 2008 *Science* **321** 385–8
[3] Balandin A A, Ghosh S, Bao W, Calizo I, Teweldebrhan D, Miao F and Lau C N 2008 *Nano Lett.* **8** 902–7
[4] Bolotin K I, Sikes K J, Jiang Z, Klima M, Fudenberg G, Hone J, Kim P and Stormer H L 2008 *Solid State Commun.* **146** 351–5
[5] Stoller M D, Park S, Zhu Y, An J and Ruoff R S 2008 *Nano Lett.* **8** 3498–502
[6] Stankovich S, Dikin D A, Dommett G H B, Kohlhaas K M, Zimney E J, Stach E A, Piner R D, Nguyen S T and Ruoff R S 2006 *Nature* **442** 282–6

[7] Eda G, Unalan H E, Rupesinghe N, Amaratunga G A J and Chhowalla M 2008 *Appl. Phys. Lett.* **93** 233502
[8] Wei T, Luo G, Fan Z, Zheng C, Yan J, Yao C, Li W and Zhang C 2009 *Carbon* **47** 2290–9
[9] Li Y, Gao W, Ci L, Wang C and Ajayan P M 2010 *Carbon* **48** 1124–30
[10] Zhou X, Huang X, Qi X, Wu S, Xue C, Boey F Y C, Yan Q, Chen P and Zhang H 2009 *J. Phys. Chem.* C **113** 10842–6
[11] Guo S, Dong S and Wang E 2010 *ACS Nano* **4** 547–55
[12] Lee J M, Pyun Y B, Yi J, Choung J W and Park W I 2009 *J. Phys. Chem.* C **113** 19134–8
[13] Wu J, Shen X, Jiang L, Wang K and Chen K 2010 *Appl. Surf. Sci.* **256** 2826–30
[14] Yao J, Shen X, Wang B, Liu H and Wang G 2009 *Electrochem. Commun.* **11** 1849–52
[15] Wang D *et al* 2010 *ACS Nano* **4** 1587–95
[16] Paek S M, Yoo E and Honma I 2009 *Nano Lett.* **9** 72–5
[17] Lambert T N, Chavez C A, Hernandez-Sanchez B, Lu P, Bell N S, Ambrosini A, Friedman T, Boyle T J, Wheeler D R and Huber D L 2009 *J. Phys. Chem.* C **113** 19812–23
[18] Wang D *et al* 2009 *ACS Nano* **3** 907–14
[19] Williams G, Seger B and Kamat P V 2008 *ACS Nano* **2** 1487–91
[20] Zhang X Y, Li H P, Cui X L and Lin Y 2010 *J. Mater. Chem.* **20** 2801–6
[21] Sun S, Gao L and Liu Y 2010 *Appl. Phys. Lett.* **96** 083113
[22] Yang N, Zhai J, Wang D, Chen Y and Jiang L 2010 *ACS Nano* **4** 887–94
[23] Tang Y B *et al* 2010 *ACS Nano* **4** 3482–8
[24] Knez M, Nielsch K and Niinistö L 2007 *Adv. Mater.* **19** 3425–38
[25] Kim H, Lee H B R and Maeng W J 2008 *Thin Solid Films* **517** 2563–80
[26] George S M 2010 *Chem. Rev.* **110** 111–31
[27] Ritala M and Leskelä M 1993 *Chem. Mater.* **5** 1174–81
[28] Aarik J, Aidla A, Uustare T, Ritala M and Leskelä M 2000 *Appl. Surf. Sci.* **161** 385–95
[29] Rahtu A and Ritala M 2002 *Chem. Vapor Depos.* **8** 21–8
[30] Xie Q, Jiang Y L, Detavernier C, Deduytsche D, Van Meirhaeghe R L, Ru G P, Li B Z and Qu X P 2007 *J. Appl. Phys.* **102** 083521
[31] Suisalu A, Aarik J, Mändar H and Sildos I 1998 *Thin Solid Films* **336** 295–8
[32] Aarik J, Aidla A, Mändar H and Sammelselg V 2000 *J. Cryst. Growth* **220** 531–7
[33] Matero R, Rahtu A and Ritala M 2001 *Chem. Mater.* **13** 4506–11
[34] Methaapanon R and Bent S F 2010 *J. Phys. Chem.* C **114** 10498–504
[35] Shin H, Jeong D K, Lee J, Sung M M and Kim J 2004 *Adv. Mater.* **16** 1197–200
[36] Lee J, Ju H, Lee J K, Kim H S and Lee J 2010 *Electrochem. Commun.* **12** 210–2
[37] Kim G M, Lee S M, Michler G H, Roggendorf H, Gösele U and Knez M 2008 *Chem. Mater.* **20** 3085–91
[38] Sander M S, Côté M J, Gu W, Kile B M and Tripp C P 2004 *Adv. Mater.* **16** 2052–7
[39] Ng C J W, Gao H and Tan T T Y 2008 *Nanotechnology* **19** 445604
[40] Tan L K, Chong M A S and Gao H 2008 *J. Phys. Chem.* C **112** 69–73
[41] Ferguson J D, Yoder A R, Weimer A W and George S M 2004 *Appl. Surf. Sci.* **226** 393–404
[42] King D M, Liang X, Zhou Y, Carney C S, Hakim L F, Li P and Weimer A W 2008 *Powder Technol.* **183** 356–63
[43] Wang X D, Graugnard E, King J S, Wang Z L and Summers C J 2004 *Nano Lett.* **4** 2223–6
[44] Hummers W S and Offeman R E 1958 *J. Am. Chem. Soc.* **80** 1339
[45] Celzard A, Mareche J F and Furdin G 2005 *Prog. Mater. Sci.* **50** 93–179
[46] Lee D W, Santos V L, Seo J W, Felix L L, Bustamante D A, Cole J M and Barnes C H W 2010 *J. Phys. Chem.* B **114** 5723–8
[47] Tang L, Wang Y, Li Y, Feng H, Lu J and Li J 2009 *Adv. Funct. Mater.* **19** 2782–9
[48] Nethravathi C, Nisha T, Ravishankar N, Shivakumara C and Rajamathi M 2009 *Carbon* **47** 2054–9
[49] Chen W, Yan L and Bangal P R 2010 *Carbon* **48** 1146–52
[50] Singh V K, Patra M K, Manoth M, Gowd G S, Vadera S R and Kumar N 2009 *New Carbon Mater.* **24** 147–52
[51] Puurunen R L 2005 *J. Appl. Phys.* **97** 121301
[52] Leskelä M and Ritala M 2003 *Angew. Chem. Int. Edn* **42** 5548–54
[53] Ritala M, Leskelä M, Nykänen E, Soininen P and Niinistö L 1993 *Thin Solid Films* **225** 288–95
[54] Aarik J, Aidla A, Sammelselg V, Siimon H and Uustare T 1996 *J. Cryst. Growth* **169** 496–502
[55] Parfitt G D 1976 *Prog. Surf. Membr. Sci.* **11** 181–226
[56] Schuisky M, Harsta A, Aidla A, Kukli K, Kiisler A A and Aarik J 2000 *J. Electrochem. Soc.* **147** 3319–25
[57] Aarik J, Aidla A, Uustare T and Sammelselg V 1995 *J. Cryst. Growth* **148** 268–75